

# Thermodynamics of tin clusters

Kavita Joshi and D. G. Kanhere

*Department of Physics, University of Pune,*

*Ganeshkhind, Pune 411 007, India*

S. A. Blundell

*Département de Recherche Fondamentale sur la Matière Condensée, CEA-Grenoble/DSM*

*17 rue des Martyrs, F-38054 Grenoble Cedex 9, France*

(Dated: February 1, 2008)

## Abstract

We report the results of detailed thermodynamic investigations of the  $\text{Sn}_{20}$  cluster using density-functional molecular dynamics. These simulations have been performed over a temperature range of 150 to 3000 K, with a total simulation time of order 1 ns. The prolate ground state and low-lying isomers consist of two tricapped trigonal prism (TTP) units stacked end to end. The ionic specific heat, calculated via a multihistogram fit, shows a small peak around 500 K and a shoulder around 850 K. The main peak occurs around 1200 K, about 700 K higher than the bulk melting temperature, but significantly lower than that for  $\text{Sn}_{10}$ . The main peak is accompanied by a sharp change in the prolate shape of the cluster due to the fusion of the two TTP units to form a compact, near spherical structure with a diffusive liquidlike ionic motion. The small peak at 500 K is associated with rearrangement processes within the TTP units, while the shoulder at 850 K corresponds to distortion of at least one TTP unit, preserving the overall prolate shape of the cluster. At all temperatures observed, the bonding remains covalent.

## I. INTRODUCTION

Clusters of the semiconducting Group IV elements are interesting not only for their potential technological applications, but also from a fundamental point of view. Small clusters of Si, Ge, and Sn have an unusual size-dependent structural evolution. Ion mobility measurements<sup>1,2,3,4</sup> revealed that for small sizes the clusters are prolate, with aspect ratios up to three, but undergo a rearrangement to a more compact, spherical form at a size of a few tens. The rearrangement is rather abrupt for Si and Ge, but more gradual for Sn. Density-functional theory (DFT) studies of ground-state structures<sup>5,6,7,8,9,10,11</sup> and optical response<sup>12</sup> confirmed the prolate shape of the small sizes and showed further that many of the ground-state structures in this size range contain the tricapped trigonal prism (TTP) unit, a nine-atom unit consisting of a triangular prism capped by one atom on each of the three side faces.

Recently, interest was focused on the thermodynamics of the prolate Sn clusters after Shvartsburg and Jarrold<sup>13</sup> found evidence, based on measurements of ionic mobility, that these clusters remain solidlike at temperatures up to at least 50 K *higher* than the melting point of bulk Sn [ $T_m(\text{bulk}) = 505$  K]. This is the only example so far observed of a small particle melting at a higher temperature than the bulk. It contradicts the standard paradigm, based on thermodynamic arguments, that a cluster should melt at a lower temperature than the bulk because of the effect of the cluster surface.<sup>14,15,16</sup> Many examples of a melting-point depression for clusters of mesoscopic size (greater than a few thousand atoms) have been demonstrated experimentally,<sup>16,17</sup> and recently a depression was also observed for small Na clusters in the size range of 50 to 200.<sup>18</sup>

There have been a few DFT studies that have implications for the thermodynamics of Sn clusters. Lu *et al.*<sup>19</sup> carried out simulated-annealing studies of  $\text{Sn}_N$  clusters ( $N \leq 13$ ), within the local-density approximation (LDA), in which the clusters were cooled from a random atomic configuration at 1980 K down to 0 K in 22 ps. By following the root-mean-square atomic displacements as a function of time, they found that the final ground-state geometries were reached roughly half way through the annealing process, at about 1000 K, for  $10 \leq N \leq 13$ . Majumder *et al.*<sup>11</sup> calculated energies of some low-lying isomeric structures within the generalized gradient approximation (GGA) for the exchange-correlation functional, and pointed out that the binding energy per atom was unusually high, only about 11% less than

that of the bulk. Finally, we studied the thermodynamics of the  $\text{Sn}_{10}$  cluster,<sup>20</sup> the smallest Sn cluster whose ground state displays the TTP unit. Using DFT in the LDA, we found the TTP unit to break up for temperatures of about 1600 K or higher, yielding a broad peak in the canonical specific heat around 2300 K.

In this paper, we revisit the thermodynamics of Sn clusters in greater detail. Prolate structures are identified in ion mobility experiments by having a smaller mobility than a spherical structure. Shvartsburg and Jarrold<sup>13</sup> observed that the mobility of  $\text{Sn}_N^+$  clusters ( $10 \lesssim N \lesssim 30$ ) remained small even at 50 K above the bulk melting point. They argued that, if the clusters had melted, they would have collapsed to a more compact, spherical form, observable by an increase in mobility, contrary to the actual observation. Now, the cluster  $\text{Sn}_{10}$ , which we studied earlier,<sup>20</sup> contains just one TTP unit and already has a compact structure both in its ground state and in high-temperature liquidlike states. Thus one would not expect to be able to detect its melting in a mobility experiment. We have therefore extended our methods to treat a cluster of twice the size,  $\text{Sn}_{20}$ . In its ground state,  $\text{Sn}_{20}$  has a prolate structure, with an aspect ratio of about 2.5, consisting of two TTP units stacked end to end. In this paper we study the structural rearrangements, caloric curve, and electronic properties of this prolate cluster, and contrast the results with those of  $\text{Sn}_{10}$ .

As in our earlier paper,<sup>20</sup> we use *ab initio* Born-Oppenheimer molecular dynamics, within the LDA of DFT, and norm-conserving pseudopotentials. This first-principles treatment of electronic structure is highly desirable, since the directional covalent bonding in small Sn clusters would be hard to describe reliably by a parametrized potential, simultaneously for the ground state and for the higher-lying isomers and liquidlike forms crucial for understanding the melting properties. Despite the computational expense of *ab initio* approaches, we obtain a sufficiently long statistical sampling of the ionic phase space as to converge the canonical specific heat to of order 10%, as extracted from a multihistogram fit. Our *total* sampling time is of order 1 ns. We believe that this statistical convergence criterion on the specific heat gives us a good sampling of the various dynamical and rearrangement processes of the cluster as a function of temperature.

As we shall see, the  $\text{Sn}_{20}$  cluster undergoes a number of dynamical processes as a function of temperature. One of these is a collapse of the prolate structure toward a more spherical, disordered structure. This collapse, which is the point where an increase in ionic mobility would be observed, occurs about 700 K above the bulk melting point in our LDA model.

Thus our calculations confirm, and explain, the experimentally observed stability of the prolate form at 50 K above the bulk melting point.<sup>13</sup> However, at lower temperatures, of order the bulk melting point or lower, we also find a large number of dynamical processes that lead to a permutational rearrangement of the atoms of the cluster, but which preserve the overall prolate shape and would therefore be unobservable in a mobility measurement.

Since we perform DFT calculations of electronic structure for every ionic configuration in our thermal ensembles, we can also study electronic properties as a function of temperature. Noting that solid bulk Sn undergoes a phase transition at 286 K between a low-temperature covalent form and a higher-temperature metallic form, we examine the bonding characteristics of the various isomers of Sn<sub>20</sub> using the electron localization function<sup>21</sup> (ELF). The bonding is found to be predominantly covalent at all temperatures considered. However, the gap between the highest occupied molecular orbital and the lowest unoccupied molecular orbital (HOMO-LUMO gap) is reduced dramatically during the collapse of the prolate structure. Finally, although we study only Sn clusters in this paper, we expect that a large number of our results would be qualitatively similar for Si and Ge clusters, since the structure and bonding of these clusters is similar to those of Sn.

The paper is organized as follows. In Sec. II we describe briefly our computational and statistical approaches. Results for the structural, caloric, and electronic properties are given in Sec. III, and the conclusions are given in Sec. IV.

## II. COMPUTATIONAL DETAILS

All the calculations have been performed using the Kohn-Sham formulation of density-functional molecular dynamics (MD),<sup>22</sup> using the nonlocal norm-conserving pseudopotentials of Bachelet *et al.*<sup>23</sup> in Kleinman-Bylander form<sup>24</sup> with the Ceperley-Alder<sup>25</sup> exchange-correlation functional. We use a cubic supercell of length 40 a.u. with an energy cutoff of 16.3 Ry, which is found to provide a convergence of the total electronic energy of better than  $10^{-6}$  a.u. To have a sufficiently precise evaluation of the Hellmann-Feynman forces on the ions, we ensure that the residual norm of each KS orbital, defined as  $|H_{\text{KS}}\psi_i - \epsilon_i\psi_i|^2$  ( $\epsilon_i$  being the eigenvalue corresponding to eigenstate  $\psi_i$  of the KS Hamiltonian  $H_{\text{KS}}$ ), was maintained at  $10^{-9}$  a.u. The ground state and other equilibrium structures have been found by carrying out several steepest-descent runs starting from structures chosen periodically

from a high-temperature simulation.

The ionic phase space is sampled by isokinetic MD,<sup>26</sup> in which the kinetic energy is held constant using velocity scaling. We split the temperature range  $150 \text{ K} \leq T \leq 3000 \text{ K}$  into about 30 different constant temperatures, performing up to 40 ps of simulation for each. We observe no evaporation on the time scale of our simulations, and therefore a reflective container (often used with classical potentials) is not explicitly required. Following the multiple-histogram (MH) method,<sup>27</sup> we then extract the classical ionic density of states  $\Omega(E)$  of the system, or equivalently the classical ionic entropy  $S(E) = k_B \ln \Omega(E)$ . With  $S(E)$  in hand, one can evaluate thermodynamic averages in a variety of ensembles. We focus in this work on the ionic specific heat and the caloric curve. In the canonical ensemble, the specific heat is defined as usual by  $C(T) = \partial U(T)/\partial T$ , where  $U(T) = \int E p(E, T) dE$  is the average total energy, and where the probability of observing an energy  $E$  at a temperature  $T$  is given by the Gibbs distribution  $p(E, T) = \Omega(E) \exp(-E/k_B T)/Z(T)$ , with  $Z(T)$  the normalizing canonical partition function. In the microcanonical ensemble, the temperature  $T(E)$  at energy  $E$  is defined following the thermodynamic definition as  $T(E) = [\partial S(E)/\partial E]^{-1}$ . The microcanonical specific heat is then defined as  $C(E) = [\partial T(E)/\partial E]^{-1}$ . More details of the extraction of thermodynamic averages can be found in our earlier work.<sup>28</sup>

The nature of the bonding can be investigated using the ELF<sup>21</sup> along with the charge density. Such ELF have been found to be extremely useful for elucidating the bonding characteristics of a variety of systems, especially in conjunction with the charge density. For a single determinantal wavefunction built from KS orbitals  $\psi_i$ , the ELF is defined as

$$\chi_{\text{ELF}} = [1 + (D/D_h)^2]^{-1}, \quad (1)$$

where

$$D_h = (3/10)(3\pi^2)^{5/3} \rho^{5/3}, \quad (2)$$

$$D = (1/2) \sum_i |\nabla \psi_i|^2 - (1/8) |\nabla \rho|^2 / \rho, \quad (3)$$

with  $\rho \equiv \rho(\mathbf{r})$  the valence-electron density. A value of  $\chi_{\text{ELF}}$  near 1 represents a perfect localization of the valence electron density.<sup>21</sup>

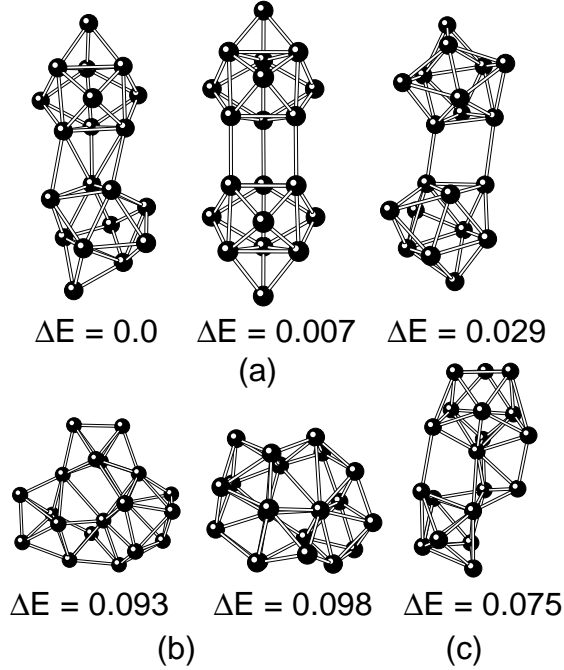


FIG. 1: (a) Some prolate equilibrium geometries having two distinct TTP units. The structure on the left is the lowest-energy structure found. (b) Nonprolate equilibrium structures found at high temperature  $T > 1250$  K. (c) Structure observed during the transition from prolate to nonprolate around  $T = 1250$  K. The excitation energy relative to the ground state is shown as  $\Delta E$ , in units of eV per atom.

### III. RESULTS AND DISCUSSIONS

We begin our discussion by presenting some equilibrium geometries of  $\text{Sn}_{20}$  (shown in Fig. 1). We distinguish two broad classes of equilibrium structures: one [Fig. 1(a)] where all the structures have a prolate shape and show the presence of two distinct TTP units, but differ in the relative orientation of the TTP units, and a second one [Fig. 1(b)] with nonprolate, compact geometries indicating that the TTP units have lost their identity. In Fig. 1(c), we also show a typical intermediate structure in which only one of the TTP units has lost its identity, but which is still prolate. The most symmetric structure (proposed as the ground state in Ref. 11) is slightly higher in energy than our lowest-energy structure. The only difference in these two structures is the relative orientation of the TTP units. Evidently, changes in the relative orientation of the TTP units give rise to several low-lying isomers [two of which are shown in Fig. 1(a)] having excitation energies of order 0.01 eV per atom

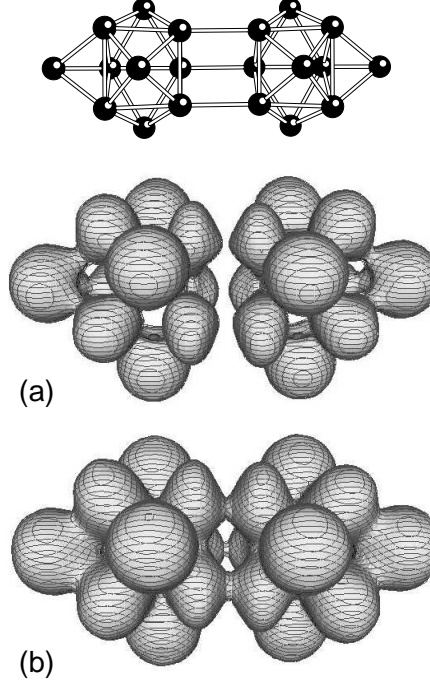


FIG. 2: Isosurfaces of the electron localization function  $\chi_{\text{ELF}}$  for a low-lying prolate form of  $\text{Sn}_{20}$  containing two TTP units; (a)  $\chi_{\text{ELF}} = 0.7$ , (b)  $\chi_{\text{ELF}} = 0.55$ .<sup>30</sup>

relative to the ground state. It is also interesting to note that a recent study<sup>29</sup> has found the most stable structure of  $\text{Si}_{20}$  to be very similar to that for  $\text{Sn}_{20}$  found in the present work.

In Fig. 1(b), we have shown two nonprolate equilibrium geometries having a difference in binding energy with respect to the ground state of about 0.1 eV per atom. These nonprolate structures are somewhat disordered, although some basic units such as tetrahedra, trigonal prisms, pentagonal bipyramids, etc., may be observed. The equilibrium structure shown in Fig. 1(c) is an intermediate structure observed during the transition from prolate to nonprolate. In this geometry, one TTP unit is intact while the other is completely destroyed. This structure is 0.075 eV higher in binding energy per atom compared to the ground state.

It is of considerable interest to investigate the nature of bonding in the  $\text{Sn}_{20}$  cluster. It may be recalled that at room temperature bulk Sn exists in a metallic phase (white tin), while in our previous work<sup>20</sup> we have shown  $\text{Sn}_{10}$  to be a covalently bonded cluster. While we therefore expect the bonding within a TTP unit in  $\text{Sn}_{20}$  to be covalent, it is interesting to examine the bonding between the TTP units. In Fig. 2 we show isosurfaces of the ELF taken at two different values of  $\chi_{\text{ELF}}$  for a typical prolate structure. Recall that a higher value of the ELF, approaching unity, indicates a localized distribution of valence electrons.

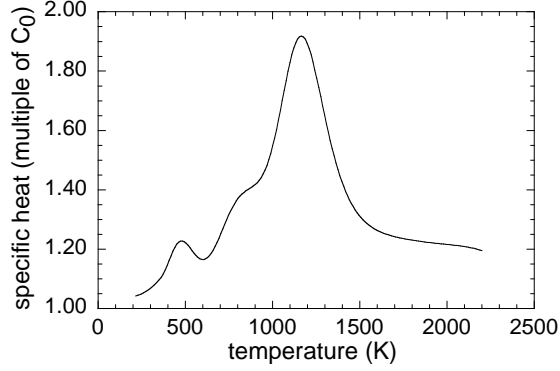


FIG. 3: Canonical specific heat of  $\text{Sn}_{20}$  cluster.  $C_0 = (3N - 9/2)k_B$  is the zero-temperature classical limit of the rotational plus vibrational canonical specific heat.<sup>28</sup>

We note that the isosurface for the higher value  $\chi_{\text{ELF}} = 0.7$ , shown in Fig. 2(a), connects the Sn ions within each TTP unit along the line joining them, implying that the ions within each TTP unit are covalently bonded. However, this higher-value isosurface of the ELF does not connect the two different TTP units. The bonds between the two TTP units are only observed at a rather lower ELF value  $\chi_{\text{ELF}} \approx 0.55$ , shown in Fig. 2(b). Evidently the two TTP units are weakly bonded to each other compared to the bonding within a TTP unit. This leads to a number of low-lying isomers with nearly degenerate energies, of which some are shown in Fig. 1(a), and which as noted above differ in the relative orientation of the TTP units.

Turning to the canonical ionic specific heat (shown in Fig. 3), we note some interesting features. First, the main peak in the specific heat, often identified with the “melting” of the cluster, occurs around 1200 K, much higher than the bulk melting point (505 K). Second, there is also a small peak around 500 K and a shoulder around 800 K. These features can be explained by examining the microscopic processes as a function of temperature. At low temperatures (below 400 K), the only motion observed is a change in the relative orientation of the two TTP units, which spans the class of low-lying isomers [Fig. 1(a)] having two distinct TTP units.

However, at around 500 K, the atoms within each TTP unit start to rearrange themselves in such a way that the TTP structure remains intact, but undergoes a reshuffling of at least three atoms in every rearrangement, including an interchange of capping atoms with atoms of the trigonal prism core. This process is similar to the one observed in  $\text{Sn}_{10}$ .<sup>20</sup> Since this



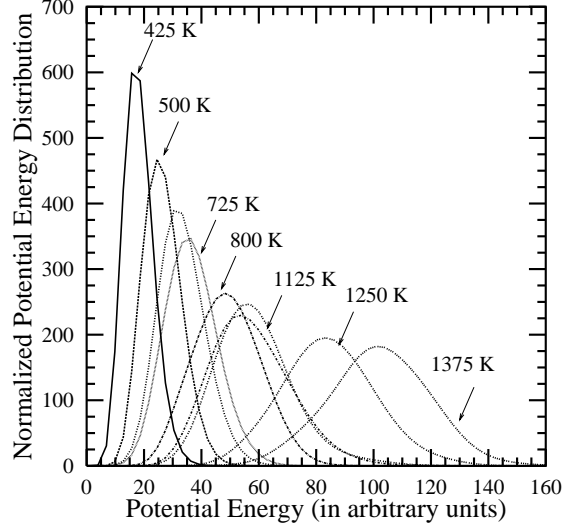


FIG. 4: Normalized potential-energy distributions for 400 K to 1375 K. The distributions are obtained from the actual data of an isokinetic sampling run at the kinetic temperature shown, but have been smoothed to suppress fluctuations and make the figure clearer.

rearrangement does not distort the TTP unit, the shape of the cluster remains prolate. The distortion of the TTP units themselves begins around 800 K. Starting at this temperature, we observe that at least one of the TTP units may be seriously distorted at various points in the dynamics, to the extent of losing its identity. The onset of these processes at 500 K and 800 K is responsible for the features seen in the canonical specific-heat curve.

This is also reflected in the potential-energy distributions (PED) for these temperatures. In Fig. 4, we show normalized PED for a series of temperatures starting at 400 K and going up to about 1300 K. Let us recall that the PED  $p(E, T)$  at temperature  $T$  follows the Gibbs distribution  $p(E, T) = \Omega(E) \exp(-E/k_B T)/Z(T)$ , where  $Z(T)$  is the canonical partition function and  $\Omega(E)$  is the density of accessible states. An examination of Fig. 4 reveals a slight relative broadening of the PED around 800 K, indicating that other modes of excitation are also available at this temperature, apart from the relative orientation of the TTP units and the internal rearrangements within the TTP units that take place at lower temperatures. This broadening is reflected in the ionic specific heat as a shoulder around 800 K.

As the temperature rises above 800 K, the relative motion between the two TTP units becomes more vigorous. The TTP units, apart from undergoing internal distortion, also

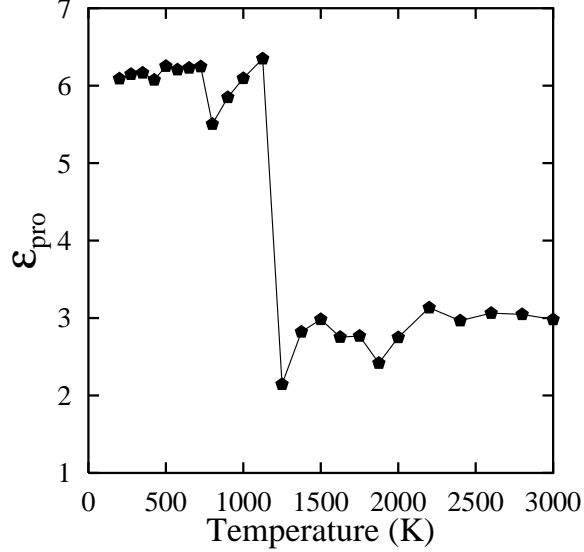


FIG. 5: The coefficient  $\epsilon_{\text{pro}}$  [see Eq. (4)] describing the degree of prolate deformation of the cluster as a function of temperature. Note the significant decrease around 1250 K.

start to come sufficiently close to one another as to initiate the exchange of atoms. This process ultimately leads at about 1200 K to the collapse of the prolate structure toward a more compact structure such as those shown in Fig. 1(b). In fact, in the temperature range 1200 to 1300 K, we occasionally observe that the collapsed structure reforms into a prolate structure. Thus the time scale at these temperatures for “hopping” between a prolate and a more compact structure is of the same order of magnitude as that of our sampling runs, namely, about 40 ps.

To summarize, there are three main modes of ionic motion observed during our simulations up to 1200 K: (i) changes in the relative orientation of two  $\text{Sn}_{10}$  units, (ii) an internal rearrangement of ions within each TTP unit, observed after 500 K, and (iii) the distortion of at least one TTP unit accompanied by the interchange of atoms between the two TTP units, observed after 800 K, leading ultimately to the fusion of the TTP units and a shape change at 1200 K.

Since it is the collapse of a prolate shape toward a more spherical shape that causes a change in the diffusion coefficient in an ion mobility experiment,<sup>13</sup> it is interesting to investigate these shape changes more explicitly. In Fig. 5, we show the thermally averaged value of the deformation coefficient  $\epsilon_{\text{pro}}$ , calculated for temperatures ranging from 200 to 3000 K, and averaged over 35 ps for each temperature. For a given ionic configuration,  $\epsilon_{\text{pro}}$

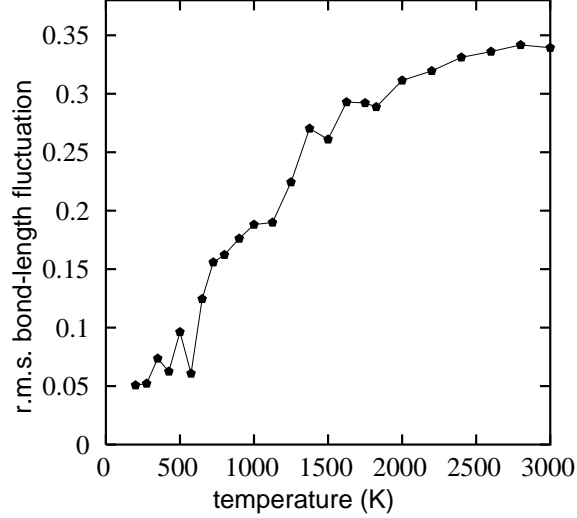


FIG. 6: The root-mean-square bond-length fluctuation  $\delta_{\text{rms}}$  [Eq. (6)] of  $\text{Sn}_{20}$ .

is defined as

$$\epsilon_{\text{pro}} = \frac{2Q_1}{Q_2 + Q_3}, \quad (4)$$

where  $Q_1 \geq Q_2 \geq Q_3$  are the eigenvalues, in descending order, of the quadrupole tensor

$$Q_{ij} = \sum_I R_{Ii} R_{Ij}. \quad (5)$$

Here  $i$  and  $j$  run from 1 to 3,  $I$  runs over the number of ions, and  $R_{Ii}$  is the  $i$ th coordinate of ion  $I$  relative to the cluster center of mass. We note that  $\epsilon_{\text{pro}}$  will be unity for a spherical cluster and greater than unity for prolate deformations. At very low temperatures, we see that  $\epsilon_{\text{pro}} \approx 6$ , corresponding to the ground-state structure in Fig. 1(a), which can be regarded roughly as having a uniaxial prolate deformation with aspect ratio  $\sqrt{\epsilon_{\text{pro}}} \approx 2.5$ . This value of  $\epsilon_{\text{pro}}$  is maintained until about 800 K, where fluctuations are observed, corresponding to the distortion of one or both TTP units, as described above. However, the cluster still maintains an overall prolate shape until about 1250 K, when there is a very sharp drop in  $\epsilon_{\text{pro}}$  toward a value of about 2 to 3, which is maintained up to temperatures of 3000 K or more. This drop corresponds to the fusion of the two TTP units to give the more spherical shapes shown in Fig. 1(b).

In discussions of cluster “melting” phenomena, it is often useful to consider the root-mean-square bond-length fluctuation  $\delta_{\text{rms}}$ , defined as

$$\delta_{\text{rms}} = \frac{2}{N(N-1)} \sum_{I>J} \frac{(\langle R_{IJ}^2 \rangle_t - \langle R_{IJ} \rangle_t^2)^{1/2}}{\langle R_{IJ} \rangle_t}, \quad (6)$$

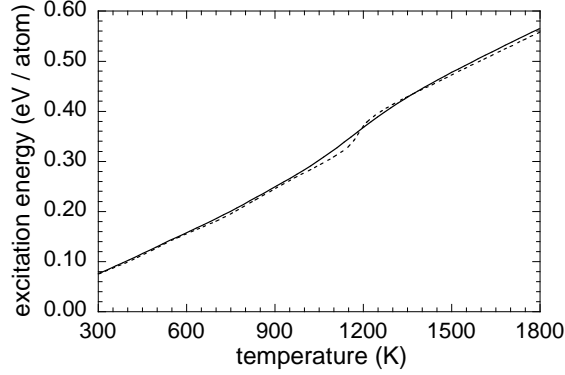


FIG. 7: The canonical (solid line) and microcanonical (dashed) caloric curves for  $\text{Sn}_{20}$ . In the microcanonical case, the temperature is defined as  $T(E) = [\partial S(E)/\partial E]^{-1}$  for excitation energy  $E$ . In the canonical case, the temperature is the heat-bath temperature, and the excitation energy is the thermally averaged excitation energy.

where  $N$  is the number of ions in the system,  $R_{IJ}$  is the distance between ions  $I$  and  $J$ , and  $\langle \dots \rangle_t$  denotes a time average over the entire trajectory. The calculated  $\delta_{\text{rms}}$  is shown in Fig. 6. It can be observed that the traditional Lindemann criterion of  $\delta_{\text{rms}} = 0.1$  signaling bulk melting is reached quite early, around 650 K. This happens because  $\delta_{\text{rms}}$  is sensitive to the permutational rearrangement of ions within a TTP unit that occurs at these temperatures. This highlights the difficulty of giving a precise definition of “melting” in a small cluster. In the temperature range 400 to 1300 K,  $\text{Sn}_{20}$  undergoes a series of complex rearrangement processes. In some sense, an individual TTP unit could be said to have melted already at 500 K, since after a sufficiently long time the reshuffling motion found at this temperature allows ions to permute throughout a TTP unit. After about 800 K, when movement of ions between the two TTP units becomes possible, ions can permute throughout the whole cluster. However, the dominant peak in the specific heat and the collapse of the overall prolate shape of the cluster do not occur until 1200 K. Note that a small step in  $\delta_{\text{rms}}$  can also be observed near 1250 K, corresponding to this collapse. In this final, collapsed state, for temperatures of 1300 K and upwards, the ionic motion is diffusive and the cluster has a highly liquidlike character.

The canonical and microcanonical caloric curves are shown in Fig. 7. The canonical curve shows a mild kink extending across the temperature range 800 to 1400 K, corresponding to the peak in the canonical specific heat in Fig. 3. The microcanonical curve has a somewhat

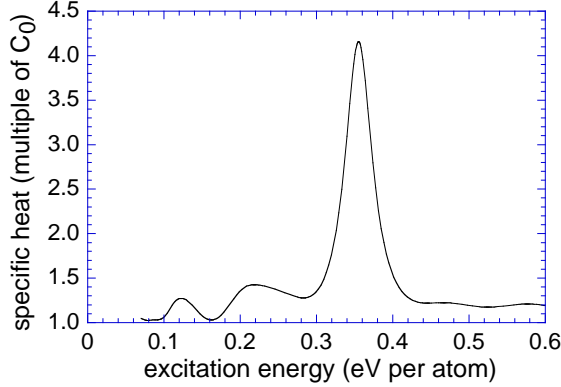


FIG. 8: The microcanonical specific heat for  $\text{Sn}_{20}$ . For  $C_0$ , see caption to Fig. 3.

more distinct step around 1250 K, but the curve does not develop an S bend, as is theoretically possible in the microcanonical ensemble.<sup>31</sup> No S bend was observed either for  $\text{Sn}_{10}$  in our previous work using the same LDA model.<sup>20</sup> As is well known, S bends for the solidlike to liquidlike transition in clusters typically occur only for special sizes, such as the complete Mackay icosahedra for the Lennard-Jones potential.<sup>27</sup> Corresponding to the absence of an S bend in the caloric curve, the microcanonical specific heat  $C(E)$ , shown in Fig. 8, is everywhere finite and positive in the energy range studied. The curve  $C(E)$  shows the same basic features as the canonical curve  $C(T)$  in Fig. 3, but with higher resolution. In particular, the shoulder at 800 K and the main peak at 1200 K in  $C(T)$  become clearly resolved in  $C(E)$  as a small peak at an excitation energy  $E = 0.22$  eV per atom and a dominant peak at 0.36 eV per atom, respectively. This allows an extraction of the effective “latent heat”  $L$  for the collapse of the prolate form,  $L \approx 0.042$  eV per atom, taken to be the area under the main peak in  $C(E)$  and above a line joining the points on the  $C(E)$  curve at  $E = 0.3$  and  $E = 0.42$  eV per atom.

Interestingly, the collapse of the prolate form around 1250 K is accompanied by a rather drastic reduction in the HOMO-LUMO gap. In Fig. 9, we show the thermal average (taken over 7.5 ps) of the HOMO-LUMO gap as a function of temperature. The gap, which is fairly constant at about 0.036 a.u. up to 1200 K, drops sharply by almost a factor of four around 1250 K, and continues to decrease as the temperature rises further. At first sight, it is tempting to interpret this reduction in the gap as related to the change in the nature of bonding from covalent to delocalized metallic.

To investigate this point in more detail, we have examined the eigenvalue spectrum of a

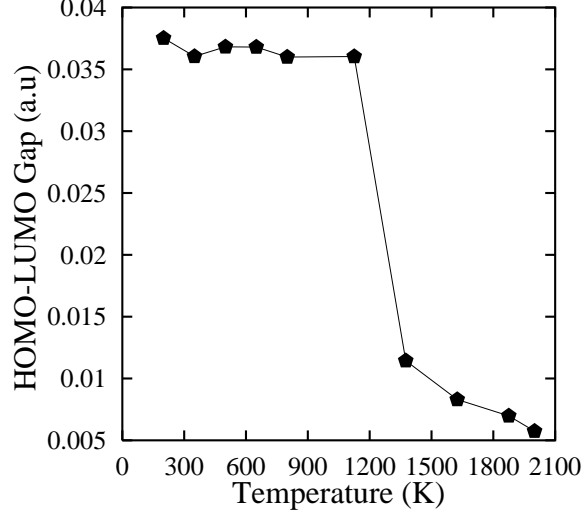


FIG. 9: The HOMO-LUMO gap, averaged over 7.5 ps, as a function of temperature.

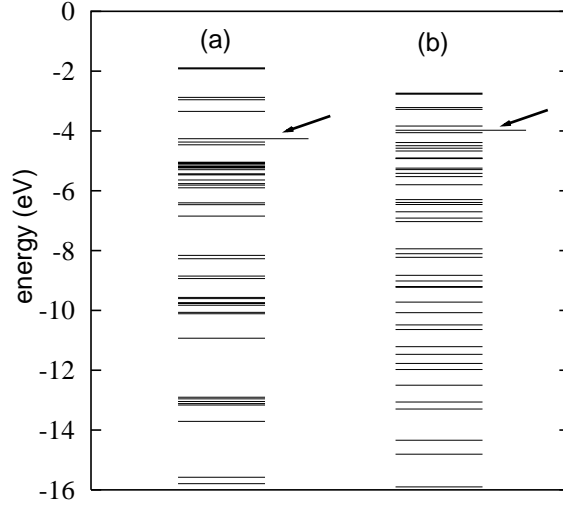


FIG. 10: The eigenvalue spectrum for (a) the ground state and (b) a nonprolate structure occurring at high temperature. The arrow indicates 40th state.

typical prolate and nonprolate structure, along with an analysis of the number of nearest neighbors of these structures. Although the nonprolate structure is more compact, the average number of nearest neighbors in both the prolate and nonprolate structures is almost the same. However, in the case of nonprolate structures, the bond angles are not optimal, resulting in strained bonds. These strained bonds can be considered to introduce disorder, which spreads out the energy levels by lifting degeneracies and splitting groupings of energy levels. This is evident from the Kohn-Sham eigenvalue spectrum [shown in Fig. 10] of a

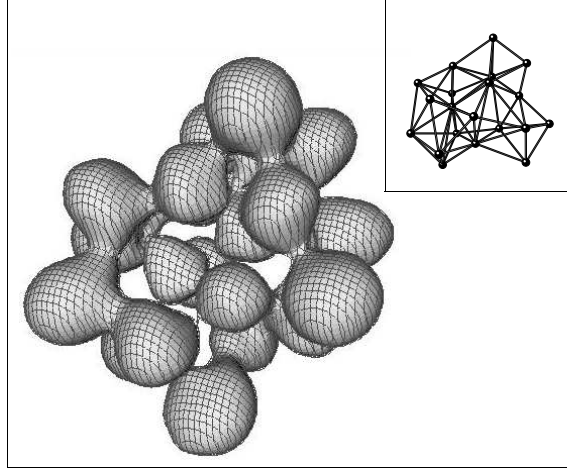


FIG. 11: Isosurface of the electron localization function  $\chi_{\text{ELF}}$  for a randomly chosen high-temperature structure of  $\text{Sn}_{20}$ .  $\chi_{\text{ELF}} = 0.7$  and the structure is shown in the inset.

prolate and nonprolate structure. Although the total occupied bandwidth is almost the same, the eigenvalue spectrum of the prolate structure shows distinct bands, in contrast to the spread-out eigenvalue spectrum of the nonprolate structure, leading to the observed substantial reduction in the HOMO-LUMO gap. To demonstrate that this reduction in the HOMO-LUMO gap is due to the disorder in the system and not to a change in the nature of the bonding, we have also examined the ELF of some randomly chosen high-temperature nonprolate structures. An isosurface of the ELF for one of these structures is shown in Fig. 11 at a value  $\chi_{\text{ELF}} = 0.7$ . Quite clearly, there is a significant localization of electron density between nearest neighbors, and the bonding is covalent.

Finally, it is interesting to note that, although in  $\text{Sn}_{20}$  the dominant peak in the specific heat occurs at a much higher temperature (1250 K) than the bulk melting point (505 K), the peak for  $\text{Sn}_{10}$  occurs at a still higher temperature (2300 K).<sup>20</sup> To understand this, we note some features of the two clusters.  $\text{Sn}_{10}$  contains one TTP unit, whereas  $\text{Sn}_{20}$  contains two. Although the nature of the bonding within each TTP unit is covalent, in  $\text{Sn}_{20}$  the two TTP units are weakly bonded to each other. When ions acquire sufficient kinetic energy, they can cross from one TTP unit to the other, and the two TTP units in  $\text{Sn}_{20}$  lose their separate identity. That is, the presence of another TTP unit provides an extra channel for ions to move. In  $\text{Sn}_{10}$ , the main peak in the specific heat is associated with the breaking of covalent bonds within the TTP unit.

In future work, it will be interesting to investigate the transition from a prolate ground

state to a nonprolate ground state as a function of cluster size.

#### IV. CONCLUSIONS

The present *ab initio* simulations on  $\text{Sn}_{20}$ , along with earlier work on  $\text{Sn}_{10}$ ,<sup>20</sup> provide insights and an explanation of the higher-than-bulk “melting point” observed experimentally.<sup>13</sup> There are two basic reasons for this behavior: (i) the covalent nature of the Sn-Sn bond in the cluster, compared to the metallic bonding of bulk Sn at room temperature, and (ii) the special stability of the TTP unit. We also note that the “melting” of a cluster as detected in an ion mobility experiment is specifically associated with the collapse of the prolate cluster shape, which requires a collapse of the TTP units themselves. Although many rearrangement processes can occur at lower temperatures, the dominant feature of the specific heat (or caloric curve) for both  $\text{Sn}_{10}$  and  $\text{Sn}_{20}$  is associated with the break up of the TTP structure. In the cluster containing one TTP unit,  $\text{Sn}_{10}$ , the TTP unit breaks up at the higher temperature, since the only processes that destroy the TTP unit are the ones that break the bonds. As the size increases, for example  $\text{Sn}_{20}$ , containing two TTP units, the collapse of the two TTP units leading to a compact cluster is aided by a relative motion between them, and occurs at a much lower temperature than the break up of the TTP unit for  $\text{Sn}_{10}$ .

In a general way, in a prolate cluster there will be a competition between the covalent bonding, which tends to favor stacks of TTP units, and the surface energy, which tends to favor more spherical structures. Our calculations reveal that for  $\text{Sn}_{20}$  the surface energy does not become the dominant factor until temperatures of about 1200 K. It is reasonable to expect that as the cluster size increases, the temperature for the collapse of the prolate structure will reduce further, until eventually the ground state structure itself is no longer prolate, as observed experimentally.



## Acknowledgments

We gratefully acknowledge the support of the Indo-French Center for the Promotion of Advanced Research under Project No. 1901-1.

---

- <sup>1</sup> M. F. Jarrold and V. A. Constant, Phys. Rev. Lett. **67**, 2994 (1991).
- <sup>2</sup> M. F. Jarrold and J. E. Bower, J. Chem. Phys. **96**, 9180 (1992).
- <sup>3</sup> J. M. Hunter, J. L. Fye, M. F. Jarrold, and J. E. Bower, Phys. Rev. Lett. **73**, 2063 (1994).
- <sup>4</sup> A. A. Shvartsburg and M. F. Jarrold, Phys. Rev. A **60**, 1235 (1999).
- <sup>5</sup> P. Jackson, I. G. Dance, K. J. Fisher, G. D. Willet, and G. E. Gadd, Int. J. Mass Spectrom. Ion Processes **157**, 329 (1996).
- <sup>6</sup> I. Vasiliev, S. Ögüt, and J. R. Chelikowsky, Phys. Rev. Lett. **78**, 4805 (1997).
- <sup>7</sup> K.-M. Ho, A. A. Shvartsburg, B. Pan, Z.-Y. Lu, C.-Z. Wang, J. G. Wacker, J. L. Fye, and M. F. Jarrold, Nature (London) **392**, 582 (1998).
- <sup>8</sup> B. Liu, Z.-Y. Lu, C.-Z. Wang, K.-M. Ho, A. A. Shvartsburg, and M. F. Jarrold, J. Chem. Phys. **109**, 9401 (1998).
- <sup>9</sup> B. Wang, L. M. Molina, M. J. López, A. Rubio, J. A. Alonso, and M. J. Stott, Ann. Phys. (Leipzig) **7**, 107 (1998).
- <sup>10</sup> A. A. Shvartsburg, B. Liu, Z.-Y. Lu, C.-Z. Wang, M. F. Jarrold, and K.-M. Ho, Phys. Rev. Lett. **83**, 2167 (1999).
- <sup>11</sup> C. Majumder, V. Kumar, H. Mizuseki, and Y. Kawazoe, Phys. Rev. B **64**, 233405 (2001).
- <sup>12</sup> J. Müller, B. Liu, A. A. Shvartsburg, S. Ögüt, J. R. Chelikowsky, K. W. M. Siu, K.-M. Ho, and G. Gantefor, Phys. Rev. Lett. **85**, 1666 (2000).
- <sup>13</sup> A. A. Shvartsburg and M. F. Jarrold, Phys. Rev. Lett. **85**, 2530 (2000).
- <sup>14</sup> P. Pawlow, Z. Phys. Chem. (Leipzig) **65**, 1 (1909).
- <sup>15</sup> K.-J. Hanszen, Z. Phys. **157**, 523 (1960); P. R. Couchman and W. A. Jesser, Nature (London) **269**, 481 (1977); K. Hoshino and S. A. Shimamura, Philos. Mag. A **40**, 137 (1979); J. Ross and R. P. Andres, Surf. Sci. **106**, 11 (1981).
- <sup>16</sup> Ph. Buffat and J.-P. Borel, Phys. Rev. A **13**, 2287 (1976).
- <sup>17</sup> For mesoscopic clusters supported on a surface, see, for example, B. T. Boiko, A. T. Pugachev,

- and V. M. Bratsykhin, *Fiz. Tverd. Tela* (Leningrad) **10**, 3567 (1968) [*Sov. Phys. Solid State* **10**, 2832 (1969)]; R. P. Berman and A. E. Curzon, *Can. J. Phys.* **52**, 923 (1974); S. J. Peppiat, *Proc. R. Soc. London A* **345**, 401 (1975).
- <sup>18</sup> M. Schmidt, R. Kusche, W. Kronmüller, B. von Issendorff, and H. Haberland, *Phys. Rev. Lett.* **79**, 99 (1997); *Nature* (London) **393**, 238 (1998).
- <sup>19</sup> Z.-Y. Lu, C.-Z. Wang, and K.-M. Ho, *Phys. Rev. B* **61**, 2329 (2000).
- <sup>20</sup> K. Joshi, D. G. Kanhere, and S. A. Blundell, *Phys. Rev. B*, **66**, 155329 (2002).
- <sup>21</sup> B. Silvi and A. Savin, *Nature* (London) **371**, 683 (1994).
- <sup>22</sup> M. C. Payne, M. P. Teter, D. C. Allen, T. A. Arias, and J. D. Joannopoulos, *Rev. Mod. Phys.* **64**, 1045 (1992).
- <sup>23</sup> G. B. Bachelet, D. R. Hamman, and M. Schlüter, *Phys. Rev. B* **26**, 4199 (1982).
- <sup>24</sup> L. Kleinman and D. M. Bylander, *Phys. Rev. Lett.* **48**, 1425 (1982).
- <sup>25</sup> D. M. Ceperley and B. J. Alder, *Phys. Rev. Lett.* **45**, 566 (1980).
- <sup>26</sup> D. J. Evans and G. P. Morriss, *Statistical Mechanics of Non-Equilibrium Liquids* (Academic Press, London, 1990).
- <sup>27</sup> A. M. Ferrenberg and R. H. Swendsen, *Phys. Rev. Lett.* **61**, 2635 (1988); P. Labastie and R. L. Whetten, *Phys. Rev. Lett.* **65**, 1567 (1990).
- <sup>28</sup> A. Vichare, D. G. Kanhere, and S. A. Blundell, *Phys. Rev. B* **64**, 045408 (2001); P. Blaise and S. A. Blundell, *Phys. Rev. B* **63**, 235409 (2001).
- <sup>29</sup> B. Li and P. Cao, *Phys. Rev. A* **62**, 023201 (2000).
- <sup>30</sup> We have examined the ELF for all the structures in Fig. 1(a) and have found them to be essentially similar.
- <sup>31</sup> T. L. Hill, *The Thermodynamics of Small Systems Part I* (Benjamin, New York, 1963); *The Thermodynamics of Small Systems Part II* (Benjamin, New York, 1963).